Nano-modulated electron beams via electron diffraction and emittance exchange for coherent x-ray generation

E.A. Nanni,[1,*] W.S. Graves,[1,†] and D.E. Moncton[1]

[1] *Massachusetts Institute of Technology, Cambridge, MA 02139, USA*

(Dated: June 24, 2015)

A new method for generation of relativistic electron beams with current modulations at nanometer scale and below is presented. The current modulation is produced by diffracting relativistic electrons in perfect crystal Si, accelerating the diffracted beam and imaging the crystal structure, then transferring the image into the temporal dimension via emittance exchange. The modulation period can be tuned by adjusting electron optics after diffraction. This tunable longitudinal modulation can have a period as short as a few angstroms, enabling production of coherent hard x-rays from a device based on inverse Compton scattering with total length of a few meters. Electron beam simulations from cathode emission through diffraction, acceleration and image formation with variable magnification are presented along with estimates of the coherent x-ray output properties.

PACS numbers:

Hard x-ray free-electon lasers (FELs) such as LCLS, SACLA, and XFEL [1–3] rely on long linear accelerators to produce high energy (> 7 GeV) electron beams that meet the resonant condition for the x-ray wavelength $\lambda_x \sim \lambda_u/\gamma^2$ for output from an undulator with period λ_u of a few centimeters and kinetic energy $E_k \approx \gamma mc^2$. The high electron energy required has the advantages of reduced space charge forces that might interfere with FEL gain and lowered electron beam geometric emittance becoming less than the diffraction-limited mode area of the coherent x-ray beam. The drawbacks are that the required facilities are large and expensive with just a few contemplated around the world, and that the electron modulation and the resulting x-ray beams produced by self-amplified spontaneous emission (SASE) are not fully coherent.

Transmission electron microscopes (TEMs) meanwhile produce a coherent spatial electron modulation at the scale of angstroms and do so using electrons with much lower energies of a few hundred keV from a compact device. This demonstrates that an ulrarelativistic beam is not *a priori* necessary for the angstrom-scale electron modulation typically produced by an x-ray FEL. Furthermore, this modulation can have a much greater coherence. We take advantage of TEM-like electron diffraction of a modestly relativistic 7 MeV electron beam in combination with a previous concept [4, 5] for transforming a spatial modulation to a coherent temporal modulation at short wavelength to produce an electron beam suitable for coherent x-ray generation. Our earlier work relied on generation of an electron beam from a nanostructured cathode that was limited to scales of hundreds of nanometers or longer. The current concept has several important advantages including potential for hard x-rays set by the atomic-scale limits of the diffracting crystal, mitigation of space charge effects due to diffraction at relativistic energy and use of a robust conventional flat cathode to produce the electrons. A hard x-ray FEL based on this technology would fit comfortably in existing industrial, academic and medical laboratories at a cost comparable to other sophisticated analytical instruments. We estimate that the output pulse will have about 10 nJ of energy compared to the millijoule levels of the large machines. However, it will be fully coherent, unlike SASE, and would be an excellent source for seeding temporally coherent x-rays from the large machines as well as directly producing new science opportunities for a broad range of applications.

Ultra-fast electron diffraction experiments using electron bunches produced by an RF photo-injector with an electron energy on the order of a few MeV and a charge of several pC [6–10] have demonstrated the feasibility of obtaining useful diffraction patterns with low emittance and high peak current electron beams. The main constraint for the use of an RF photo-injector for electron diffraction is the ability to achieve a low enough emittance or angular spread of the incoming electron bunch. Additionally, the diffraction or phase contrast image must be preserved through the imaging optics.

In the present case we model a 1 pC electron bunch photoemitted from a flat cathode in a 3.5 cell RF gun operating at 9.3 GHz with a peak cathode field of 170 MV/m and RF phase of 80^o at emission with PARMELA [11]. The electron bunch is generated by a UV laser pulse with 30 fs full width and a parabolic spatial distribution with RMS size of 30 μm in order to produce a 3-dimensional ellipsoid in blow-out mode [12, 13]. The normalized emittance is

$$\varepsilon_{xn} = \frac{1}{m_e c}\sqrt{\langle x^2\rangle \langle p_x^2\rangle - \langle x p_x\rangle^2} \tag{1}$$

where x is the transverse coordinate, p_x is the transverse momentum, m_e is the electron mass and c is the speed of light, with an initial value $\varepsilon_{xn} = 9$ nm-rad, which is an aggressive assumption but is supported by recent measurements [14]. The gun exit energy is 4.5 MeV. A short

20 cm linac then accelerates the beam to 7 MeV and removes its time-energy chirp. A solenoid magnet surrounding the gun collimates the electron beam resulting in an RMS spot size at the crystal of $\sigma_x = 101$ μm with an angular distribution $\sigma_{x'} = 7.7$ μrad which is more than one order of magnitude smaller than the Bragg angle. Simulation results show bunch length expansion to an RMS length of 100 fs with a peak current of 3.2 A.

For a perfect Si crystal with a lattice spacing of $a = 5.43$ Å we can see from Bragg's law, $\lambda = 2d_{\rm hkl}\sin\theta$ where λ is the electron wavelength and $d_{\rm hkl}$ are the interplanar spacings, that for the lowest order diffracted beam (hkl = 111) $2\theta = 0.305$ mrad with respect to the incident electron beam. This small diffraction angle proves advantageous as it limits aberrations in the downstream electron optics. The sample thickness, t, required for the 111 diffraction beam is given by the normalized amplitude $|\varphi|^2 = \sin^2\left(\frac{\pi t}{\xi}\right)$, where $\xi = 1.35$ μm is the extinction length given by $\xi = \frac{\pi V_c}{\lambda F}$ with a structure factor of $F = 22.6$ Å and $V_c = (0.543\ \text{nm})^3$.

The scattering geometry is shown in Fig. 1(a) with $\vec{k} + \vec{g} = \vec{k'} + \vec{s}$, where k is the momentum vector for the incident electron, k' is the momentum of a diffracted electron, $g = 2\pi/d_{111}$ is the reciprocal lattice vector and s is the deviation vector. Due to the finite emittance of the electron bunch, it is not possible for all the k vectors of the incident particles to be properly aligned with the crystal plane, resulting in a a decreased probability of interacting with the crystal lattice for increasing s.

For clarity we will only consider the two beam case for a target consisting of a uniform medium. In practice, higher-order scattering events will be present requiring adjustments to sample dimensions and collection optics (bright-field vs dark-field). Targets consisting of layered materials can also be considered to produce the desired beam.

The intensity of the diffracted beam is

$$I = \frac{\sin\left(z s_{\rm eff}/2\right)^2}{\xi^2 s_{\rm eff}^2} \tag{2}$$

where $s_{\rm eff} = \sqrt{s^2 + (2\pi/\xi)^2}$ and $I_0 = 1 - I$ is the intensity of the forward beam[15]. The forward and diffracted beams for a uniform thickness perfect Si crystal are shown in Fig. 1(b).

One approach to producing modulation in the electron bunch is to use a grating, Fig. 2(a). From (2) we can see that varying the thickness, z, in x results in spatially alternating intensities of I_0 and I, *i.e.* diffraction contrast. The limitation on this modulation period is set by the minimum feature size that can be fabricated, however note that the image produced by the diffracted electron beam may be significantly demagnified to reach shorter periods. Subsequently, one of the two beams (I_0, I) could be blocked and the remaining beam would be

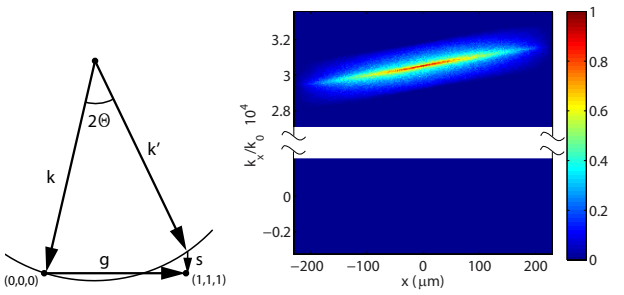

(a) (b)

FIG. 1: (a) Scattering geometry for an incident particle and (b) the calculated diffraction for the electron bunch from the RF photo-injector for $t = \xi/2$ with 98% of the beam undergoing one scattering event (upper panel). Remaining electrons (lower panel) did not scatter.

sent through emittance exchange (EEX) optics [16–20]. The bunching factor, defined as

$$b_{0x} = \frac{1}{N_e}\sum_{p=1}^{N_e} e^{ikx_p} \tag{3}$$

where N_e is the number of electrons, x_p is the transverse position of the p^{th} particle, $k = 2\pi/\lambda_x$, and λ_x is the period of modulation, is a useful measure of how well phased the modulation is at a particular wavelength. For a random assortment of particles (no modulation) $b_{0x} = 1/\sqrt{N_e} \ll 1$. For the modeled case with a grating period of 150 nm, the forward scattered beam (Fig. 2(b)) contains 0.35 pC and has a bunching factor $|b_{0x}| = 0.76$ (Fig. 2(c)). The transverse modulation of either beam undergoes demagnification which can be varied and then is imaged into the longitudinal dimension via EEX. We have recently shown [21] that emittances with ratios as high as 10^4 between longitudinal and transverse dimensions can be fully exchanged. If both beams are imaged without aberrations the modulation would disappear.

The full accelerator setup is shown in Fig. 2(d) including the interaction area where coherent x-rays would be produced via inverse Compton scattering (ICS) of a high power laser or THz field on the modulated electrons. A test case was analyzed for diffraction from a grating with 150 nm period and demagnification factor of 1/120 to produce a 1.24 nm modulation period which would produce coherent 1 keV x-rays. Diffraction contrast modulation with the Si structure and dimensions shown in Fig. 2(a) was used. After striking the Si grating the forward scattered beam is accelerated in a short x-band linac from 7 MeV to 22.5 MeV. The accelerator is described in [22] and the arrangement of the EEX line is given in [21, 23]. The imaging quadrupole lenses are set up as a telescope that demagnifies the beam by a factor of 1/14, and then the EEX line further demagnifies by a factor of 1/6. These demagnification factors in combination with the modest demagnification due to accelera-

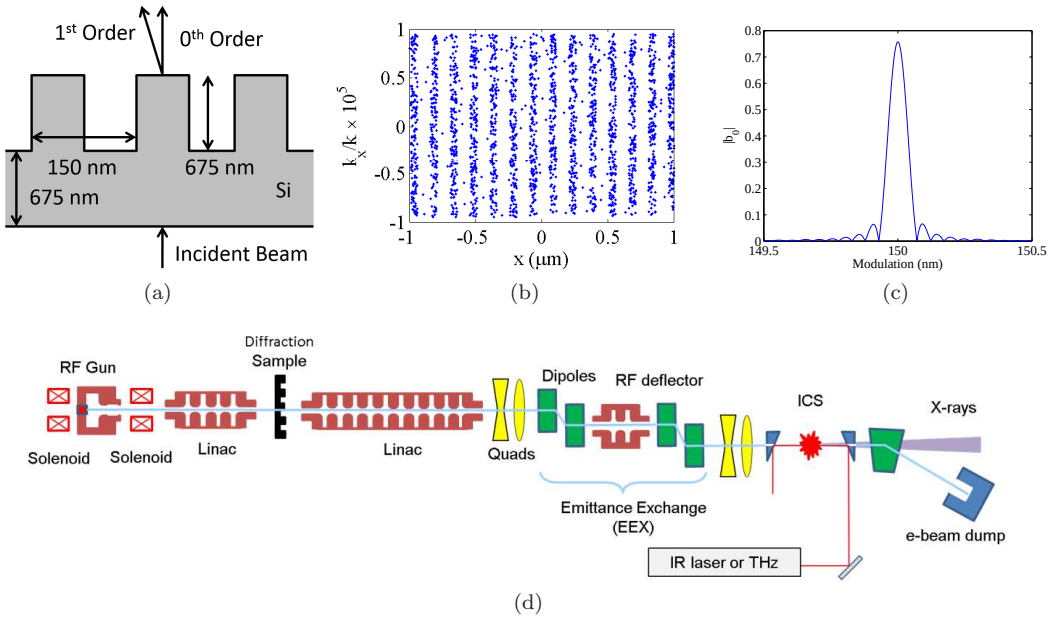

FIG. 2: (a) The Si grating. (b) The forward scattered (0^{th} order) electron beam and (c) the calculated b_0 with ∼150 nm spacing. (d) Schematic of the compact coherent x-ray source with RF photo-injector, electron diffraction crystal, X-band linac, EEX line and ICS laser interaction area. Entire assembly is approximately 4 m long.

tion result in a 1.24 nm modulation at the EEX output. Fig. 3(a) shows the imaged pattern of the Si grating after being accelerated and magnified with $b_0 = 0.61$ for the entire electron bunch. The bunching factor calculated locally as a function of transverse coordinates is shown in Fig. 3(b).

We can estimate the 1 keV x-ray performance by treating the ICS interaction as an effective undulator field and applying the universal FEL scaling formulas of Xie [24]. The electron spot size at the crystal results in scattering from about 1800 grooves thus producing 1800 nanobunches after EEX for a total electron bunch length of 8 fs with peak current 47 A. The high-power IR laser pulse used for ICS is equivalent to a static undulator in this x-ray performance estimate. This is physically correct if the laser field is uniform, a challenging issue for which solutions [25–27] have been proposed. For an IR laser with 10 μm wavelength and strength parameter $a_0 = 0.4$, electron beam Twiss parameter $\beta_x = 2$ mm, normalized transverse emittance $\epsilon_{xn} = 10$ nm, and energy spread $\Delta E/E = 5 \times 10^{-5}$, the effective Pierce parameter including the effects of emittance, diffraction, and energy spread [28] is $\rho = 3.2 \times 10^{-4}$, the exponential gain length is $L_g = 401$ μm, and the saturated power is 810 kW. Only 2-3 gain lengths are required to reach saturation because the electrons are bunched before interacting with the laser, allowing use of a few ps laser pulse. Furthermore because the energy spread is an order of magnitude smaller than the Pierce parameter, the saturation power could be substantially exceeded by using a chirped laser pulse equivalent to a tapered undulator.

In order to extend the electron bunch modulation into the hard x-ray regime (*i.e.* sub-nm modulation) without significant amounts of demagnification, phase-contrast imaging of diffracted electrons can directly provide modulation on the order of the atomic structure spacing (∼ 5 Å). Phase-contrast imaging relies on the interference of the diffracted beam, ϕ, with the forward scattered beam, ϕ_0:

$$\varphi_0(r) = \varphi_0(z)\, e^{i\vec{k_0}\cdot\vec{r}} \tag{4}$$

$$\varphi(r) = \varphi(z)\, e^{i\left(\vec{k_0}+\vec{g}\right)\cdot\vec{r}} \tag{5}$$

The amplitude of these two wavefunctions is determined by the excitation of two Bloch waves (ψ_1, ψ_2) at the entrance of the crystal and the relative phase of these two Bloch waves at the exit of the crystal. As the electron bunch arrives at the Si crystal, no modulation is present in the beam and its wavefunction is a plane wave with a flat phase front. Once the electron penetrates into the crystal it can no longer be described as a plane wave, because the Si atoms act as potential wells and apply a spatially varying phase advance. The Bloch waves (ψ_1, ψ_2) are the new eigenstates for the electron, and the incident plane wave excites these two waves with equal amplitude for $\vec{s} = 0$. Note that (ψ_1, ψ_2) propagate colinearly, but they have unique wavevectors $(k^{(1)}, k^{(2)})$ or $(\vec{k} + \gamma^{(1)}\hat{z}, \vec{k} + \gamma^{(2)}\hat{z})$. When the electrons exit the crystal we once again can describe them as plane waves with modulated phases. However, depending on the relative phase and amplitude of the two Bloch waves, two

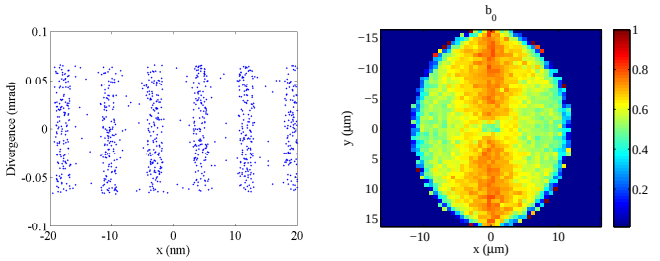

(a) (b)

FIG. 3: (a) Individual electrons imaged after magnification and acceleration at the entrance of the EEX line. (b) The bunching factor as a function of the transverse position in the beam.

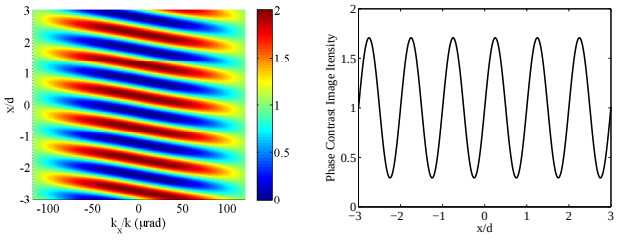

(a) (b)

FIG. 4: (a) Phase-contrast modulation as a function of incident angle and transverse position. (b) Integrated phase-contrast modulation over the incident electron distribution ($\sigma_{x'} \approx 50$ μrad) at the exit of the Si crystal.

diffracted plane waves can be excited (ϕ_0, ϕ). At the crystal exit the two waves are

$$\phi_0(z) = e^{isz/2}\left[\cos\left(\frac{s_{\text{eff}}z}{2}\right) - i\cos\left(\cot(s\xi)^{-1}\right)\sin\left(\frac{s_{\text{eff}}z}{2}\right)\right] \quad (6)$$

$$\phi(z) = ie^{isz/2}\sin\left(\cot(s\xi)^{-1}\right)\sin\left(\frac{s_{\text{eff}}z}{2}\right) \quad (7)$$

noting that in $\widehat{x}$ both waves contain modulation in phase on the order of g. We can describe the total beam image as

$$I_{tot} = (\varphi_0 + \varphi)(\varphi_0 + \varphi)^*, \quad (8)$$

which becomes

$$\begin{aligned} I_{\text{tot}} &= 1 + 2\sin\left(\cot(s\xi)^{-1}\right)\sin\left(\frac{s_{\text{eff}}z}{2}\right) \\ &\times\left[\sin(gx)\cos\left(\frac{s_{\text{eff}}z}{2}\right)\right. \\ &+\cos(gx)\cos\left(\cot(s\xi)^{-1}\right) \\ &\left.\times\sin\left(\frac{s_{\text{eff}}z}{2}\right)\right]. \end{aligned} \quad (9)$$

We evaluate this expression for a sample depth of 338 nm or $\xi/4$ which results in the optimal mix (50/50) of the forward and diffracted beam. Fig. 4(a) is the intensity of the diffraction pattern in the transverse coordinate for varying incident angle and (b) is the accumulated population for our design case focused to a RMS spot size at the crystal of $\sigma_x = 11.5$ μm with angular distribution $\sigma_{x'} \approx 50$ μrad to reduce the number of modulation periods. Excellent phase contrast is observed at the exit of the Si crystal.

Phase-contrast imaging has not yet been demonstrated with RF photo injectors, however the electron bunch produced by a state-of-the-art RF gun has sufficient beam quality as shown in the previous section. Imaging the transverse modulation at the interaction point will require careful analysis of aberrations from the optical elements in the setup. We estimate the effects of aberrations with analytical calculations that assume imaging with a standard objective lens. For phase contrast we must consider the wave-optical formulation of aberrations due to imaging. In the wave-optical formulation the effect of aberrations is given by a phase shift $W(\theta) = 2\pi\Delta s/\lambda$ where Δs is the change in optical path with respect to the ideal spherical wave front. The phase shift can result from three effects: spherical aberrations, fluctuations in the thickness of the sample, or change in focal length due to energy. These effects combine to give a total phase shift of

$$W(\theta) = \frac{\pi}{2\lambda}\left(C_s\theta^4 - 2(\Delta f - \Delta a)\theta^2\right) \quad (10)$$

where $\Delta f = f\Delta E/E$ and Δa is the variation of the longitudinal position of the sample (effectively due to tilt) and should be kept to on the order of Δf. It is sufficient to keep Δa on the order of 40 nm (with an illumination spot of 11.5 μm this is a tilt of 4 mrad), which is a weaker tolerance than the required 0.1 mrad alignment for the crystal plane.

Observing modulation of the electron beam that is on the order of the lattice spacing $a = 5.43$ Å requires the ability to collect electrons from a transverse momentum space that covers $k_\perp = 4\pi/a$ or $k_\perp/k_0 = 0.5$ mrad which includes a minimum of two diffraction peaks. To analyze the imaged beam we take the amplitude distribution at the output of the crystal $\phi(r, z_{out}) = \phi_0(r, z_{out}) + \phi(r, z_{out})$ and propagate it as spherical wave fronts to the image location [29] including aberrations from (10). The aberrations and imaged electron beam are shown in Fig. 5 assuming that the sample is placed a distance $S_1 = 2f$ from the objective lens. Fig. 5(b) shows that a strong modulation is possible for the given beam and transport conditions.

In conclusion, we have presented detailed calculations showing how to produce a moderately relativistic electron beam that is coherently modulated at a nanometer scale in preparation for generating fully coherent x-rays.

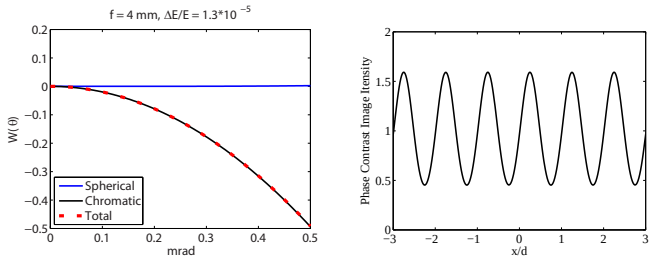

(a) (b)

FIG. 5: (a) Added phase as a function of the angle of divergence. (b) Electron population in phase-contrast image propagated through a lens with a focal length of 4 mm for the initial conditions in Fig. 4(b).

Furthermore, we have presented a method to extend the technique to sub-nanometer modulation using phase contrast electron diffraction that would enable generation of coherent hard x-rays. Using conventional ICS from a laser pulse, electron beams prepared in this manner can be a stable source of powerful fully coherent x-rays from a table-top source. Such a source would have many impacts, enabling labs and groups around the world access at modest cost to the remarkable science produced by ultrashort pulse coherent x-rays. The output pulse energy is modest due to the low charge employed, yet the temporal coherence and resulting spectral purity are likely to open new applications that are not achievable with SASE-based XFELs. The coherent power significantly exceeds the startup noise in a SASE FEL and could be a stable coherent seed source to improve the performance of large facilities.

* Now at SLAC National Accelerator Laboratory, Menlo Park, CA 94025, USA
† Now at Arizona State University, Tempe, Arizona 85287, USA

[1] P. Emma, R. Akre, J. Arthur, R. Bionta, C. Bostedt, J. Bozek, A. Brachmann, P. Bucksbaum, R. Coffee, F.-J. Decker, et al., nature photonics **4**, 641 (2010).
[2] D. Pile, Nature Photonics **5**, 456 (2011).
[3] M. Altarelli, R. Brinkmann, M. Chergui, W. Decking, B. Dobson, S. Düsterer, G. Grübel, W. Graeff, H. Graafsma, J. Hajdu, et al., Technical Design Report, DESY **97**, 1 (2006).
[4] W. Graves, F. Kärtner, D. Moncton, and P. Piot, Physical review letters **108**, 263904 (2012).
[5] W. Graves, K. Berggren, S. Carbajo, R. Hobbs, K. Hong, W. Huang, F. Kärtner, P. Keathley, D. Moncton, E. Nanni, et al., Proceedings of the 2013 FEL Conference, New York, USA (2013).
[6] Y. Murooka, N. Naruse, S. Sakakihara, M. Ishimaru, J. Yang, and K. Tanimura, Applied Physics Letters **98**, 251903 (2011).
[7] J. Hastings, F. Rudakov, D. Dowell, J. Schmerge, J. Cardoza, J. Castro, S. Gierman, H. Loos, and P. Weber, Applied physics letters **89**, 184109 (2006).
[8] P. Musumeci, J. Moody, and C. Scoby, Ultramicroscopy **108**, 1450 (2008).
[9] M. Hada, J. Hirscht, D. Zhang, S. Manz, K. Pichugin, D. Mazurenko, S. Bayesteh, H. Delsim-Hashemi, K. Floettmann, M. Huening, et al., in *International Conference on Ultrafast Structural Dynamics* (Optical Society of America, 2012), pp. JT2A–47.
[10] R. D. Miller, Annual review of physical chemistry (2014).
[11] L. Young and J. Billen, Tech. Rep., LA-UR-96-1835 (2003).
[12] O. Luiten, S. Van der Geer, M. De Loos, F. Kiewiet, and M. Van Der Wiel, Physical review letters **93**, 094802 (2004).
[13] P. Musumeci, J. T. Moody, R. J. England, J. B. Rosenzweig, and T. Tran, Phys. Rev. Lett. **100**, 244801 (2008), URL `http://link.aps.org/doi/10.1103/PhysRevLett.100.244801`.
[14] T. Li, B. L. Rickman, and W. A. Schroeder, Journal of Applied Physics **117**, 134901 (2015).
[15] A. Howie, Philosophical Magazine **14**, 223 (1966).
[16] M. Cornacchia and P. Emma, Phys. Rev. ST Accel. Beams **5**, 084001 (2002).
[17] P. Emma, Z. Huang, K.-J. Kim, and P. Piot, Phys. Rev. ST Accel. Beams **9**, 100702 (2006).
[18] Y.-E. Sun, P. Piot, A. Johnson, A. Lumpkin, T. Maxwell, J. Ruan, and R. Thurman-Keup, Physical review letters **105**, 234801 (2010).
[19] B. E. Carlsten, K. A. Bishofberger, S. J. Russell, and N. A. Yampolsky, Phys. Rev. ST Accel. Beams **14**, 084403 (2011).
[20] D. Xiang and A. Chao, Phys. Rev. ST Accel. Beams **14**, 114001 (2011).
[21] E. A. Nanni and W. S. Graves, arXiv preprint arXiv:1503.03493 (2015).
[22] W. Graves, J. Bessuille, P. Brown, S. Carbajo, V. Dolgashev, K.-H. Hong, E. Ihloff, B. Khaykovich, H. Lin, K. Murari, et al., Phys. Rev. ST Accel. Beams **17**, 120701 (2014).
[23] E. Nanni, W. Graves, and P. Piot, in *2014 International Particle Accelerator Conference* (2014), pp. 1952–1955.
[24] M. Xie, Nucl. Inst. Meth. A **445**, 59 (2000).
[25] C. Chang, J. Liang, D. Hei, M. F. Becker, K. Tang, Y. Feng, V. Yakimenko, C. Pellegrini, and J. Wu, Opt. Express **21**, 32013 (2013).
[26] D. Seipt, S. G. Rykovanov, A. Surzhykov, and S. Fritzsche, Phys. Rev. A **91**, 033402 (2015).
[27] J. E. Lawler, J. Bisognano, R. A. Bosch, T. C. Chiang, M. A. Green, K. Jacobs, T. Miller, R. Wehlitz, D. Yavuz, and R. C. York, Journal of Physics D: Applied Physics **46**, 325501 (2013).
[28] R. Bonifacio, C. Pellegrini, and N. L, Opt. Commun. **50**, 373 (1984).
[29] L. Reimer and H. Kohl, *Transmission electron microscopy: physics of image formation*, vol. 36 (Springer Science & Business Media, 2008).